

See discussions, stats, and author profiles for this publication at: <https://www.researchgate.net/publication/44693248>

Vibrational Analysis of Amino Acids and Short Peptides in Hydrated Media. VII. Energy Landscapes, Energetic and Geometrical Features of L -Histidine with Protonated and Neutral Sid...

ARTICLE *in* THE JOURNAL OF PHYSICAL CHEMISTRY B · JULY 2010

Impact Factor: 3.3 · DOI: 10.1021/jp103348y · Source: PubMed

CITATIONS

16

READS

17

3 AUTHORS:



Fernando Pfluger

Université Paris 13 Nord

23 PUBLICATIONS 330 CITATIONS

[SEE PROFILE](#)



Belén Hernández

Université Paris 13 Nord

39 PUBLICATIONS 375 CITATIONS

[SEE PROFILE](#)



Mahmoud Ghomi

Université Paris 13 Nord

112 PUBLICATIONS 1,774 CITATIONS

[SEE PROFILE](#)

Vibrational Analysis of Amino Acids and Short Peptides in Hydrated Media. VII. Energy Landscapes, Energetic and Geometrical Features of L-Histidine with Protonated and Neutral Side Chains

Fernando Pflüger, Belén Hernández, and Mahmoud Ghomi*

Groupe de Biophysique Moléculaire, UFR Santé-Médecine-Biologie Humaine (SMBH), Université Paris 13, 74 rue Marcel Cachin, 93017 Bobigny cedex, France

Received: April 14, 2010; Revised Manuscript Received: May 28, 2010

In manuscript VI of the same series (*J. Phys. Chem. B* 2010, 114, 1077–1088), we reported the geometrical and vibrational features of lysine and arginine, that is, two α -amino acids (α -AAs) with positively charged side chains, at physiological conditions. Here, we report our results on histidine, one of the most biologically important α -AAs, whose side chain can be neutral or positively charged through a protonation–deprotonation process of the nitrogens involved in its cyclic side chain at pH values in the physiological range. We have recorded at room temperature Raman scattering and Fourier-transform infrared (FT-IR) absorption spectra from the aqueous solutions of the AA at pH values 4, 6.8, and 8. It has been shown that a Raman spectrum recorded at the intermediate pH (6.8) can be perfectly reconstituted by a linear combination of those observed at two extreme pH values (4 and 8), allowing determination of the populations of histidine with protonated and neutral side chains in solution. The above-mentioned experimental data were completed by the vibrational spectra recorded in D_2O . On the other hand, quantum mechanical calculations at the DFT/B3LYP/6-31++G* allowed us to analyze the energetic, geometrical, and vibrational features of histidine. Through a discussion on the basis of experimental and theoretical results, we comment on (i) the potential energy surfaces of histidine placed in a polarizable dielectric continuum, providing molecular energy landscapes as a function of its side chain orientations around $C_\alpha-C_\beta$ and $C_\beta-C_\gamma$ bonds; (ii) the full geometry optimization of the low energy conformers placed in a solvent continuum or in the presence of n explicit water molecules ($n = 3, 7$); (iii) the energy value separating the two histidine forms with neutral side chains; (iv) the determination of the side chain pK_a by means of Raman spectra; and (v) the assignment of the observed vibrational modes by means of the lowest-energy conformers of hydrated histidine.

I. Introduction

Histidine (His or H) is a conditionally essential AA and should consequently be provided by the daily diet.^{1,2} Thanks to its special features, His can be classified among the α -AAs with cyclic or positively charged side chains. In fact, the His side chain contains a heterocyclic aromatic ring (imidazole) linked to the C_β atom (Figure 1). At physiological conditions, this ring can adopt neutral and protonated forms, with a higher trend to be neutral. Two neutral tautomers exist for the imidazolic ring, depending on the location of the proton on its N_δ or N_e atoms. When the side chain is positively charged, both of these nitrogens are protonated (Figure 1).

Because of its particular chemical constitution, His is considered as one of the most biologically important AAs: (i) The role of His residues in globular proteins, such as myoglobin^{3,4} and hemoglobin,^{5,6} being capable of oxygen binding, should be stressed. Two His residues, always spaced by 29 other AAs, in a myoglobin chain, or in one of the tetrameric hemoglobin chains, take part in the oxygen binding process of these proteins. One of these histidines, named *proximal*, is directly bound to the iron atom located at the center of the porphyrinic ring, whereas the other one, named *distal*, interacts with an oxygen molecule bound to the iron atom. Both of these contacts are apparently established through the N_e atom of proximal and

distal histidines. (ii) In all serine proteases,⁷ such as chymotrypsin, trypsin, and elastase,^{8,9} the so-called *catalytic triad* is based on a cooperative mechanism of three AAs: His, Asp, and Ser, located at the 57, 102, and 195 positions of the enzyme, respectively. Through this mechanism, chymotrypsin^{10,11} cleaves the peptide chains at the C-terminal of Trp, Tyr, Phe, Leu, and Met substrates, that is, residues with large size hydrophobic side chains.^{12–14} In this context, the role of His57 is to maintain the spatial structure of the triad within the enzyme active site by the intermediate of H-bonds (through N_δ and N_e atoms) with the terminal groups of Asp102 and Ser195 side chains. (iii) Several His residues are highly conserved in all known types of hydrogenases, that is, enzymes catalyzing the reversible oxidation of hydrogens. In fact, electrons are transferred from the active site of the enzyme to the redox partner through a pathway of iron/sulfur clusters in which at least two His residues are involved.^{15–17}

Optical spectroscopic methods have shown their ability to achieve a rapid and efficient search of a peptide chain secondary conformations in the aqueous phase. For instance, in manuscripts II, III, and V of the present series,^{18–20} we have shown the extent to which the joint use of circular dichroism and Raman scattering can lead to the establishment of the structure–activity relationship in short cationic minimalist peptides used for DNA delivery inside living cells^{18,19} or in somatostatin, a 14-mer cyclic peptide hormone with important physiological activity.²⁰ In parallel with our experimental works on the short peptides with therapeutic

* To whom correspondence should be addressed. E-mail: mahmoud.ghomi@univ-paris13.fr.

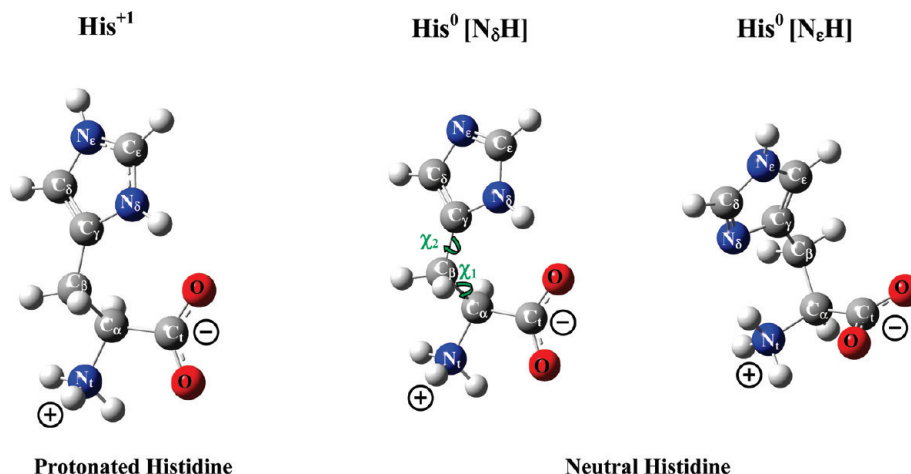


Figure 1. L-Histidine with a zwitterionic backbone and a protonated or a neutral side chain. His⁺¹ (left) refers to the form with a protonated side chain (1+ extra charge). His⁰[N_δH] (middle) and His⁰[N_εH] (right), with only one hydrogen present on the N_δ and N_ε atoms, respectively, correspond to the forms with neutral side chains. Conformational angles χ_1 (N_t-C_α-C_β-C_γ) and χ_2 (C_α-C_β-C_γ-N_δ) allows the orientation of the side chain ring with respect to the backbone to be defined.

interest, we have initiated in manuscripts I, IV, and VI of the present series^{21–23} a systematic investigation by means of FT-IR, Raman spectra, and quantum mechanical calculations their constituting AAs in hydrated media. This combined methodology has been applied to glycine²¹ as well as to other AAs with hydrophobic (Ala, Val, Ileu, Leu)^{21,22} and positively charged (Lys, Arg)²³ side chains. Here, our aim is to focus on histidine. It is to be emphasized that the experimental part of the present work takes benefit of the previous studies on (i) Raman and IR spectra of His-HClO₄ and L-His.HBF₄ crystals²⁴ and (ii) IR^{25–27} and Raman^{27,28} spectra of histidine in aqueous solutions. From the theoretical point of view, we were inspired from the recently published in vacuo quantum mechanical calculations at the self-consistent field and density functional theory (DFT) levels for analyzing the so-called potential energy surfaces (PES) and hypersurfaces of *N*-formyl-L-histidinamide in its cationic, neutral, and anionic forms.^{29–33} Together, all our observed and theoretical data in this report attempt to bring insight into the energy landscapes as a function of side chain conformation as well as the geometrical and vibrational features of histidine with neutral and protonated side chains in hydrated media.

II. Materials and Methods

II.1. Experimental Section. L-Histidine lyophilized powder was purchased from Sigma-Aldrich and dissolved either in water taken from a Millipore filtration system or in D₂O (100% purity) provided by Euriso-top (Saclay, France). To avoid D₂O/H₂O exchange, deuterated samples were prepared under dry air atmosphere. The pH of prepared solutions was estimated with an accuracy of $\sim\pm 0.1$. Measured pH after dissolving directly powder sample in H₂O was ~ 8 . Lower pH values (6.8 and 4) could be reached by gradual addition of HCl. Because the water solubility of histidine is $\sim 4.2\%$ w/w at 25 °C, the saturated solution thus has a concentration of ~ 270 mM. For Raman scattering measurements, the selected concentration was 50 mM, well below the saturated solution concentration. Consequently, the obtained Raman spectra well correspond to histidine aqueous solution and resemble those previously published.^{27,28}

Stokes Raman components were collected by exciting 50 μ L of solution, placed in suprasil quartz cells (5 mm path length), with the 488 nm line emitted by an Ar⁺ laser (Spectra Physics). Light scattered at a right angle was analyzed on a Jobin-Yvon T64000 spectrograph in a single spectrograph configuration with

a 1200 grooves/mm holographic grating and a holographic notch filter. A liquid-nitrogen-cooled CCD detection system (Spectrum One, Jobin-Yvon) based on a Tektronix CCD chip of 2000 \times 800 pixels was used to collect Raman data. Accumulation time for each Raman spectrum was 20 min, and the effective spectral slit width was set to ~ 5 cm⁻¹.

Transmission FT-IR spectra were recorded on a Bruker Tensor 27 spectrophotometer under continuous dry air purge. Histidine solution was placed between two circular ZnSe windows separated by a Teflon spacer of 25 μ m. However, in the case of the saturated solutions used for FT-IR absorption, we have paid attention to avoid recording spectra from the eventually precipitated histidine, which may appear as a suspension in solution.²⁶ Our FT-IR spectra resemble those obtained by Mesu et al.²⁷ Each infrared spectrum corresponds to 20 scans and was collected with 1 cm⁻¹ spectral resolution and a Blackman–Harris 3-terms apodization function. FT-IR data were collected using Opus software delivered by Bruker.

Postprocessing of Raman and FT-IR spectra, including subtraction of the buffer contribution, baseline correction and smoothing, was performed by means of GRAMS/32 software (Galactic Industries). To facilitate the comparison between the different vibrational spectra, each of them has been normalized to its most intense band. Final presentation of vibrational spectra has been performed by means of SIGMAPLOT package.

II.2. Theoretical. As mentioned in section I, a histidine side chain can adopt neutral and cationic (protonated) forms at the pH values close to the physiological one. Hereafter, for the sake of brevity, the two tautomers of histidine with neutral side chains are referred to as: His⁰[N_δH] or His⁰[N_εH], where the superscript 0 means neutral, and the content of the bracket shows whether the hydrogen is bound to the ring N_δ or N_ε nitrogen. His⁺¹ abbreviates histidine with a positively charged (protonated) side chain, in which both the above-mentioned nitrogens are evidently bound to hydrogens (Figure 1).

Structural and vibrational data of His⁰[N_δH], His⁰[N_εH] and His⁺¹ forms were estimated by means of DFT calculations.³⁴ The hybrid B3LYP functional (i.e., Becke's three parameter (B3) exchange functional³⁵ with the Lee–Yang–Parr non local correlation functional³⁶) and standard split valence double- ζ Gaussian atomic basis sets containing diffuse functions on heavy and hydrogen atoms (i.e., 6-31++G*) were used. Numerical calculations were performed with the Gaussian03 pakage.³⁷

TABLE 1: Main Geometric and Energetic Features of the Low-Energy Conformers of Histidine with Neutral and Protonated Side Chains^a

	χ_1	χ_2	conformer	E_e	E_v	E_{tot}	ΔE
His + continuum							
His ⁺¹	-156.0	-53.4	tg^-	-549.289 39	108.258	-549.116 87	0.00
	-64.5	-67.6	g^-g^-	-549.288 31	107.649	-549.116 76	+0.07
	69.6	67.5	g^+g^+	-549.287 11	108.218	-549.114 65	+1.39
	-163.6	59.0	tg^+	-549.285 73	107.663	-549.114 16	+1.70
	64.1	-112.7	g^+t	-549.286 01	107.869	-549.114 11	+1.73
	52.4	46.0	g^+g^+	-549.283 33	108.265	-549.110 80	+3.81
His ⁰ [N _e H]	-61.0	53.9	g^-g^+	-548.837 36	100.457	-548.677 27	0.00
	58.0	-55.1	g^+g^-	-548.836 59	100.480	-548.676 46	+0.51
	-62.0	-60.1	g^-g^-	-548.833 32	100.018	-548.673 93	+2.10
	50.6	67.4	g^+g^+	-548.831 17	100.094	-548.671 66	+3.52
	52.2	64.1	g^+g^+	-548.830 79	100.112	-548.671 25	+3.78
	-170.6	71.6	tg^+	-548.830 75	100.212	-548.671 05	+3.90
His ⁰ [N _δ H]	-61.6	-67.4	g^-g^-	-548.831 95	100.076	-548.672 42	0.00
	61.6	80.5	g^+g^+	-548.830 79	100.439	-548.670 73	+1.06
	57.4	-107.3	g^+g^-	-548.829 77	100.293	-548.669 94	+1.56
	-154.0	-57.6	tg^-	-548.830 01	100.662	-548.669 59	+1.78
	-172.4	91.9	tg^-	-548.828 94	100.264	-548.669 16	+2.05
	-160.7	58.5	tg^+	-548.827 21	100.008	-548.667 83	+2.88
His + 3H ₂ O							
His ⁺¹	-161.9	-48.5	tg^-	-778.504 70	156.438	-778.255 40	0.00
	66.2	60.6	g^+g^+	-778.499 78	157.420	-778.248 91	+4.07
	104.7	-62.1	g^+g^-	-778.493 86	158.750	-778.240 88	+9.11
	119.0	-67.6	g^+g^-	-778.491 30	157.931	-778.239 75	+9.82
His ⁰ [N _e H]	-61.4	52.3	g^-g^+	-778.117 51	149.755	-777.878 86	0.00
	47.3	-67.4	g^+g^-	-778.114 23	149.559	-777.875 89	+1.86
	-153.0	97.4	tg^+	-778.106 10	149.435	-777.867 96	+6.84
	-165.2	141.7	tt	-778.104 89	149.447	-777.866 73	+7.61
	7.6	68.3	g^+g^+	-778.103 54	149.782	-777.864 85	+8.79
His ⁰ [N _δ H]	52.3	71.4	g^+g^+	-778.113 91	150.099	-777.87471	0.00
	-156.3	-63.8	tg^-	-778.110 74	149.515	-777.872 47	+1.41
	-32.3	89.1	g^-g^+	-778.108 21	149.759	-777.869 55	+3.24
	-58.8	-75.2	g^-g^-	-778.106 80	149.330	-777.868 83	+3.69
	55.5	-105.5	g^+g^-	-778.100 30	149.337	-777.862 31	+7.78
	-167.1	100.4	tg^+	-778.096 37	149.955	-777.859 00	+9.86
His + 7H ₂ O							
His ⁺¹	-159.0	-48.7	tg^-	-1084.276 76	218.868	-1083.927 97	0.00
	102.3	-73.0	g^+g^-	-1084.274 09	219.559	-1083.924 20	+2.36
	172.1	70.9	tg^+	-1084.274 59	220.793	-1083.922 73	+3.29
	-159.9	-90.6	tg^-	-1084.269 82	218.348	-1083.921 86	+3.83
	66.8	64.1	g^+g^+	-1084.270 78	219.176	-1083.921 50	+4.06
	163.4	56.5	tg^+	-1084.268 07	218.341	-1083.920 12	+4.93
His ⁰ [N _e H]	61.0	-86.4	g^+g^-	-1083.887 06	212.993	-1083.547 63	0.00
	-156.6	81.6	tg^+	-1083.882 50	212.090	-1083.544 51	+1.96
	-156.9	88.7	tg^+	-1083.882 54	212.529	-1083.543 86	+2.37
	60.0	-88.9	g^+g^-	-1083.880 64	212.253	-1083.542 40	+3.28
	-153.2	95.1	tg^+	-1083.877 30	212.091	-1083.539 32	+5.21
	-99.4	79.2	g^-g^+	-1083.875 54	211.724	-1083.538 14	+5.95
	-108.8	74.4	g^-g^+	-1083.875 10	211.735	-1083.537 68	+6.24
His ⁰ [N _δ H]	-148.0	-55.4	tg^-	-1083.879 61	212.155	-1083.541 51	0.00
	-81.5	-70.3	g^-g^-	-1083.878 78	212.131	-1083.540 73	+0.49
	52.0	71.5	g^+g^+	-1083.880 14	213.006	-1083.540 69	+0.51
	-49.7	93.2	g^-g^+	-1083.875 51	212.152	-1083.537 42	+2.57
	161.1	65.5	tg^+	-1083.869 47	213.335	-1083.529 50	+7.54
	180.0	39.8	tg^+	-1083.863 37	210.994	-1083.527 13	+9.02

^a His⁰[N_eH] and His⁰[N_δH] correspond to the forms with a neutral side chain, whereas His⁺¹ abbreviates the form with a protonated side chain. See Figure 1 for more details and the definition of χ_1 and χ_2 conformational angles. g^+ , g^- and t refer to χ_1 and χ_2 angles. E_e (hartrees), E_v (kcal/mol) and E_{tot} (hartrees) correspond to electronic, zero-point vibrational, and total energies, respectively. ΔE (kcal/mol) is the energy difference with respect to the lowest energy conformer, whose energy is set to zero. See stereoviews of the lowest energy conformers ($\Delta E = 0$) derived from each hydration model (continuum, 3H₂O, 7H₂O) in Figures 3–5.

As far as the hydration treatment of histidine is concerned, two different theoretical approaches were considered: (i) an implicit hydration by means of a polarizable dielectric continuum model,^{38,39} basically capable of mimicking a bulk water environment around the molecule, and (ii) an explicit hydration by the intermediate of a cluster of n water molecules, where n

should be a minimal number, but also a significant one, capable of building an acceptable H-bond network between water and all the acceptor (N, COO⁻) and donor (NH₃⁺, NH) sites of the host molecule (Figure 1).

On the basis of a series of in vacuo quantum mechanical calculations on *N*-formyl-L-hisdinamide, it has been previously

TABLE 2: Effect of Implicit and Explicit Hydrations on a Selection of Calculated Vibrational Modes in Histidine with Neutral and Protonated Side Chains^a

His ⁺		His ⁰ [N _e H]		His ⁰ [N _δ H]		tentative assignments
continuum	7H ₂ O	continuum	7H ₂ O	continuum	7H ₂ O	
Backbone Vibrations						
3332, 3309	3320, 3171	3359, 3311	3397, 3142	3356, 3312	3248, 3213	NtH ₃ ⁺ asym. st.
3260	2922	3134	3083	3233	3040	NtH ₃ ⁺ sym. st.
1639	1646	1615	1667	1642	1655	COO ⁻ asym. st.
1338	1437	1401	1422	1359	1433	COO ⁻ sym. st.
1650, 1604	1765, 1754	1657, 1643	1754, 1689	1656, 1606	1754, 1750	NtH ₃ ⁺ asym. bend.
1491	1646	1489	1576	1468	1640	NtH ₃ ⁺ sym. bend.
Side Chain Vibrations						
3233	3329	3307	3418			N _e -H st.
3207	2862			3297	3458	N _δ -H st.

^a His⁰[N_eH] and His⁰[N_δH] correspond to the forms with neutral side chains. His⁺ abbreviates histidine with a protonated side chain (Figure 1). See stereoviews of the lowest-energy conformers used for these vibrational calculations in Figures 3 and 5.

discussed^{29–33} that the conformation of a histidine residue involved in a peptide chain depends basically on four torsion angles: φ , ψ (backbone), and χ_1 , and χ_2 (side chain). When histidine is considered as an isolated AA, φ and ψ torsion angles are not as important as they are in a peptide backbone because they describe only the orientation of the terminal COO⁻ and NH₃⁺ charged groups with respect to C_α atom. Energy landscapes, represented by the variation of the electronic energy (E_e) of histidine, embedded in a dielectric continuum, as a function of χ_1 and χ_2 torsion angles, were drawn. To obtain a sufficiently smooth PES of $E_e(\chi_1, \chi_2)$, electronic energy was calculated by a single point approach through successive variations of 15° at each step of χ_1 or χ_2 . The most prominent conformers corresponding to the deepest valleys of these energy landscapes were subject to full geometry optimization. Then we proceeded to further calculations in the presence of n explicit water molecules. To get a better estimation of the relative energy of different optimized conformers, obtained either in an implicit solvent or in the presence of explicit water molecules, we considered their total energies $E_{\text{tot}} = E_e + E_v$, with $E_v = 1/2 \sum \hbar\nu$, representing the zero-point vibrational energy, where \hbar is the Plank constant and ν is the frequency of one of the $3N - 6$ vibrational modes. Here, N represents either the number of the atoms of an isolated AA (embedded in the continuum) or the total number of atoms included in a cluster formed by an AA and its surrounding water molecules.

As in our previous works on AAs,^{21–23} we have used the raw calculated wavenumbers, without the application of any scaling factor, to assign the observed ones (Tables 2–5). This strategy leads to a better estimation of the inaccuracies related to the theoretical level, basis sets, and the neglect of anharmonic effects. The scaling factors can be easily determined by the ratios $r = \nu_{\text{exp}}/\nu_{\text{calc}}$, where ν_{calc} is a calculated wavenumber allowing to assign an observed mode whose wavenumber is ν_{exp} . As can be found from Tables 3–5, the r values are quite close to the unity for all the assigned vibrational modes. The assignment of the calculated harmonic modes was performed on the basis of the PED (potential energy distribution) matrix as expressed in terms of a combination of local symmetry and internal coordinates by means of a homemade program.

III. Results and Discussion

Our previous calculations have confirmed the stability of the zwitterionic form of an AA embedded in a dielectric continuum.²³ In contrast, in the presence of explicit hydration, several previous theoretical calculations have shown that at least

three water molecules are needed for avoiding the proton transfer from NH₃⁺ to COO⁻ groups of an AA backbone.^{40–43} In the course of our recent calculations on different AAs,^{21–23} we have emphasized that the optimal number of hydration (n) can be, in fact, equal to the number of H-bond donors and acceptors of a given AA. Thus, it has been verified that five water molecules are necessary to adequately hydrate an AA backbone, that is, its terminal NH₃⁺ and COO⁻ groups. As far as the His side chain is concerned, the imidazolic ring possesses two sites (N_δ and N_e) that are capable of forming H-bonds with water, either as a donor or an acceptor, depending on the imidazolic ring form: His⁰[N_δH], His⁰[N_eH], and His⁺ (Figure 1). Following these criteria, we have undertaken our calculations by two different n values: (i) $n = 3$, minimal value for maintaining the zwitterionic character of the AA backbone, and (ii) $n = 7$ (for maintaining zwitterionic character and reproducing H-bond interactions of the backbone and side chain with surrounding water molecules).

III.1. Scan of the Energy Landscapes of Histidine Embedded in a Continuum Solvent. Figure 2 displays the PES of histidine with neutral and protonated side chains. Each PES presents the variation of electronic energy in a 15 kcal/mol energy range beginning from the lowest value taken as reference. We particularly focus on the (χ_1, χ_2) map regions, where PES minima are located. The PES of His⁰[N_δH] reveals two valleys, narrow along the χ_1 axis, that is, centered principally around g⁺ and g⁻ regions of this angle, but extended along the χ_2 axis, including the quasi-whole g⁺, t, and g⁻ regions. Two other localized minima are found in tg⁺ and tg⁻ regions of the (χ_1, χ_2) map. The situation is different in His⁰[N_eH], where three localized valleys are found in g⁺g⁻, g⁻g⁺ and g⁻g⁻ regions. The PES of His⁺ resembles that of the His⁰[N_δH] form (Figure 2), with more extended valleys in the tg⁺ and tg⁻ regions of the (χ_1, χ_2) map.

III.2. Search of Low Energy Conformers of Histidine in a Continuum Solvent. On the basis of the location of the valleys in the energy landscapes (Figure 2, see also section III.1 for details), we have carried out full geometry optimization of a representative set of conformers belonging to these regions of the (χ_1, χ_2) maps. Table 1 reports the most prominent geometrical and energetic features of the optimized conformers with protonated and neutral side chains. For each form, there are six distinct conformers located in a 4 kcal/mol interval (ΔE) from the lowest energy conformer ($\Delta E = 0$). The lowest energy conformer of His⁺ is a tg⁻ one (Figure 3 top), facilitating the H-bond interaction of the side chain N_δH and the backbone

TABLE 3: Vibrational Modes of Histidine with a Protonated Side Chain in Aqueous Solutions (H_2O) and Their Assignments^a

Raman pH 4	IR pH 4	calcd His ⁺¹ /cont	assignments (PED %)	calcd His ⁺¹ /7w	assignments (PED %)
1632 (s)	1628 (s)		CtOO ⁻ asym. st. (26), C γ -C δ (19) NtH ₃ ⁺ asym. bend. (47), NtH ₃ ⁺ asym. bend. (25)	1667 1650 1639 1604	NH ₃ ⁺ asym. bend. (48), HOH (16), NtH ₃ ⁺ asym. bend (11) NH ₃ ⁺ asym. bend. (24), W(HOH) (21), CtOO ⁻ asym. st. (12) C γ -C δ (15), C γ -N δ -H (10), W(HOH) (10) NtH ₃ ⁺ sym. bend. (18), NtH ₃ ⁺ sym. rock. (17), CtOO ⁻ asym. st. (10)
1495 (s)	1438 (w)		N δ -C ε (26), N ε -C ε -H (12), N δ -C ε -H (10) N ε -C ε (20), C ε -N ε -H (17), C δ -N ε -H (12)	1524 (s)	N δ -C ε (27), N ε -C ε -H (13), N δ -C ε -H (10) C ε -N ε -H (26), C δ -N ε -H (20), C ε -N ε (13)
1440 (m)			C β -bend. (36), NH ₃ ⁺ sym. bend. (25), NH ₃ ⁺ sym. rock. (22)	1491 1485 1445	C β -bend. (34), NH ₃ ⁺ sym. bend. (18), NH ₃ ⁺ sym. rock. (16) C γ -N δ (16), N δ -C ε (12), C ε -N δ -H (11)
1415 (m)	1414 (sh)		CtOO ⁻ sym. st. (21), Nt-C α -H (19), C β -rock. (18), OCtO (11)	1405 (sh)	C ε -N δ -H (15), C γ -C δ (14), C β -rock. (11), N δ -C ε (11), C ε -N δ -H (10)
1364 (m)	1362 (sh)		CtOO ⁻ sym. st. (25), C β -C α -H (21), OCtO (21), C β -twist. (10)	1419 1384 1367 1338 1311 1288 1266 (w) 1237 (w)	C β -rock. (36), Nt-C α -H (34) CtOO ⁻ sym. st. (28), C β -twist. (22), CaCtOO ⁻ sym. bend. (18) C γ -N δ (18), C β -C γ (11), Ct-C α -H (11) C γ -N ε (22), N ε -C δ -H (16), C γ -C δ -H (16), C β -rock. (10) C β -twist. (47), Ct-C α -H (12)
1346 (m)	1346 (m)		N ε -C ε (22), N ε -C ε -H (20), N δ -C ε -H (18), C ε -N ε -H (12)	1198 (s)	N ε -C ε (22), N ε -C ε -H (20), N δ -C ε -H (18), C ε -N ε -H (12) NtH ₃ ⁺ asym. rock. (33), Ca-C β (22), C β -C α -H (17)
1335 (m)	1328 (sh)		C ε -N δ -H (21), C γ -N δ -H (19), N δ -C ε (14), C γ -C δ -H (11)	1189 (m)	NtH ₃ ⁺ asym. rock. (33), N δ -C ε -H (10); C γ -C δ -H (10), N δ -C ε -H (10)
1278 (sh)	1298 (w)		C γ -N ε (29), N ε -C δ -H (22)	1153 (m)	C β -twist. (27), NH ₃ ⁺ asym. rock. (12)
1270 (s)	1279 (w)		NtH ₃ ⁺ asym. rock. (49), CaCtOO ⁻ sym. bend. (15), Ct-C α -H (11)	1094 (m)	C β -Ca-H (17); NtH ₃ ⁺ asym. rock. (14), C ε -N ε (12)
			Nt-C α (37), C β -wag. (12), C α -C β (11)	1096 (m)	N δ -C ε (13), N δ -C ε -H (14), C ε -N ε (12)
			N α -C α -H (15), C γ -N δ -C ε (14), C β -C γ (10), C γ -C δ (10)	1077 (w)	C γ -N ε (33), N ε -C δ -H (24)
			CaCtOO ⁻ sym. bend. (21), NtH ₃ ⁺ asym. rock. (20), C α -C β (18), C β -wag. (15)	1055 (w)	N δ -C ε (14), C α -C β (10)
			C ε -N ε -C δ (17), OCtO (15)	994 (m)	N α -C α -H (15), C γ -N δ -C ε (14), C β -C γ (10), C γ -C δ (10)
			Nt-C α (16), C β -wag. (16), NtH ₃ ⁺ asym. rock. (14)	962 (sh)	N δ -C ε (14), C ε -N ε -C δ (17); C β -scissor. (14)
			N τ (C ε -N δ) (45), ω (C δ -H) (27), τ (N δ -C γ) (14)	923 (w)	N δ -C ε (14), C ε -N ε -C δ (17); C β -scissor. (14)
			C α CtOO ⁻ sym. bend. (80), C α -C τ (10), C β -wag. (10)	921 (w)	N δ -C ε (14), C ε -N ε -C δ (17); C β -scissor. (14)
			ω (C ε -H) (51), ω (C δ -H) (25), OCtO (11)	927	N δ -C ε (14), C ε -N ε -C δ (17); C β -scissor. (14)
			ω (C ε -H) (42), ω (C δ -H) (41), τ (C δ -C γ) (17)	904	N δ -C ε (14), C ε -N ε -C δ (17); C β -scissor. (14)
			OCtO (95)	889 (sh)	N δ -C ε (14), C ε -N ε -C δ (17); C β -scissor. (14)
			τ (N ε -C ε) (37), τ (C δ -N ε) (24), ω (N ε -H) (18), τ (C ε -N δ) (14)	883 (w)	N δ -C ε (14), C ε -N ε -C δ (17); C β -scissor. (14)
			τ (C δ -N ε) (37), OCtO (18), ω (N δ -H) (18), τ (C ε -N δ) (14)	798	N δ -C ε (14), C ε -N ε -C δ (17); C β -scissor. (14)
			ω (N ε -H) (79)	766	N δ -C ε (14), C ε -N ε -C δ (17); C β -scissor. (14)
			τ (C δ -N ε) (37), OCtO (18), ω (N δ -H) (18), τ (C ε -N δ) (14)	731	N δ -C ε (14), C ε -N ε -C δ (17); C β -scissor. (14)
			ω (N ε -H) (79)	679	N δ -C ε (14), C ε -N ε -C δ (17); C β -scissor. (14)
			τ (C δ -N ε) (37), OCtO (18), ω (N δ -H) (18), τ (C ε -N δ) (14)	654	N δ -C ε (14), C ε -N ε -C δ (17); C β -scissor. (14)
			ω (N ε -H) (79)	616	N δ -C ε (14), C ε -N ε -C δ (17); C β -scissor. (14)

^a s, intense; m, medium; w, weak; sh, shoulder; Raman, Raman spectra recorded in H₂O (Figure 6); IR, FT-IR spectra recorded in H₂O (Figure 7); Caled, calculated wavenumbers from the lowest-energy conformers of histidine with a protonated side chain. His⁺¹/cont calculated data obtained by means of a solvent continuum (Figure 3 top). His⁺¹/7w calculated data obtained from histidine interacting with seven water molecules (Figure 5, top). The angular bending modes of the tetrahedrons located on the C β atom of the side chain are referred to as bending (-bend), wagging (-wag), twisting (-twist), rocking (-rock), and scissoring (-scissor). ω and τ designate an out-of-plane bending or a torsional internal coordinate, respectively.

TABLE 4: Vibrational Modes of Histidine with Neutral Side Chains in Aqueous Solutions (H_2O) and Their Assignments^a

Raman pH 8	IR pH 8	calcd $\text{His}^0[\text{N}_t\text{H}]$	assignments (PED%)	calcd $\text{His}^0[\text{N}_d\text{H}]$	assignments (PED%)
1627 (w)	1754	NtH_3^+ asym. bend. (32), NtH_3^+ asym. bend. (14)	1754	NH_3^+ asym. bend. (42)	
	1689	W(HOH) (29), NH_3^+ asym. bend. (18), CtOO^- asym. st. (17)	1750	NH_3^+ asym. bend. (41), W(HOH) (10)	
	1667	CtOO^- asym. st. (53)	1655	CtOO^- asym. st. (54), W(HOH) (27)	
1573 (s)	1582 (s)	$\text{C}_\gamma-\text{C}\delta$ (32), $\text{N}_\varepsilon-\text{C}\delta-\text{H}$ (16), $\text{C}\delta-\text{N}_\varepsilon-\text{H}$ (10), $\text{C}\beta-\text{C}_\gamma$ (10)	1604	$\text{C}_\gamma-\text{C}\delta$ (23), $\text{C}\beta-\text{C}_\gamma$ (13), $\text{N}\delta-\text{C}_\gamma-\text{C}\delta$ (11)	
	1518 (s)	NtH_3^+ sym. bend. (30), NtH_3^+ sym. rock. (28), $\text{N}\delta-\text{C}_\varepsilon$ (25), $\text{N}_\varepsilon-\text{C}_\varepsilon-\text{H}$ (19), $\text{C}_\varepsilon-\text{N}_\varepsilon-\text{H}$ (14)			
1495 (s)	1502	$\text{C}\beta$ -bend. (56)	1516	$\text{N}\varepsilon-\text{C}\varepsilon$ (24), $\text{N}\delta-\text{C}\varepsilon-\text{H}$ (12), $\text{N}_\varepsilon-\text{C}\varepsilon-\text{H}$ (11)	
	1496	$\text{C}\beta$ -bend. (37), $\text{N}_\varepsilon-\text{C}_\varepsilon$ (14), $\text{C}\delta-\text{N}_\varepsilon-\text{H}$ (12)	1501	$\text{C}\beta$ -bend. (87)	
1441 (s)	1440 (m)	CtOO^- sym. st. (25), $\text{C}\alpha-\text{C}\varepsilon$ (14), $\text{C}\beta$ -rock. (11)	1445	$\text{Nt}-\text{C}\alpha-\text{H}$ (12), CtOO^- sym. st. (11), $\text{C}\beta$ -rock. (11)	
	1412 (s)	$\text{Nt}-\text{C}\alpha-\text{H}\alpha$ (33), $\text{C}\beta-\text{C}\alpha-\text{H}$ (23), $\text{C}\beta$ -rock. (22)	1433	CtOO^- sym. st. (15), $\text{C}_\gamma-\text{C}\delta$ (12), $\text{C}_\varepsilon-\text{N}_\delta-\text{H}$ (11), $\text{N}\delta-\text{C}\varepsilon$ (10)	
1410 (s)	1399	$\text{N}\delta-\text{C}\varepsilon$ (20), $\text{C}\beta$ -twist. (16), $\text{C}_\gamma-\text{N}\delta$ (12)	1400	$\text{Nt}-\text{C}\alpha-\text{H}\alpha$ (22), $\text{C}\beta-\text{C}\alpha-\text{H}\alpha$ (11)	
	1374	CtOO^- sym. st. (21), $\text{Nt}-\text{C}\alpha-\text{H}$ (19), $\text{C}\beta$ -rock. (15)	1394	CtOO^- sym. st. (20), $\text{Nt}-\text{C}\alpha-\text{H}\alpha$ (12), $\text{N}\varepsilon-\text{C}\varepsilon$ (10)	
1357 (s)	1363	$\text{C}\beta$ -rock. (48), $\text{C}\beta-\text{C}\alpha-\text{H}\alpha$ (10)	1387	$\text{C}\beta$ -rock. (48), $\text{C}\beta-\text{C}\alpha-\text{H}\alpha$ (10)	
	1345 (s)	CtOO^- sym. st. (14), NtH_3^+ asym. rock. (14), $\text{C}\beta$ -rock. (14), $\text{C}\beta-\text{C}\alpha-\text{H}$ (12)	1350	CtOO^- sym. st. (14), NtH_3^+ asym. rock. (14), $\text{C}\beta$ -rock. (14), $\text{C}\beta-\text{C}\alpha-\text{H}$ (12)	
1324 (s)	1328	NtH_3^+ asym. rock. (24), $\text{C}\beta$ -rock. (15), $\text{C}\varepsilon-\text{C}\alpha-\text{H}$ (10)	1287	$\text{N}\varepsilon-\text{C}\varepsilon-\text{H}$ (25), $\text{N}\delta-\text{C}\varepsilon-\text{H}$ (12), $\text{C}\beta$ -twist. (12), $\text{N}\varepsilon-\text{C}\delta-\text{H}$ (11)	
	1287 (s)	$\text{C}_\gamma-\text{N}\delta$ (14), $\text{C}_\gamma-\text{C}\delta-\text{H}$ (11)	1271	$\text{C}_\gamma-\text{N}\varepsilon$ (28), $\text{C}_\gamma-\text{C}\delta-\text{H}$ (15), $\text{C}\beta-\text{C}_\gamma$ (12), $\text{N}\alpha-\text{C}\delta-\text{H}$ (10)	
1268 (sh)	1283 (sh)	$\text{N}\delta-\text{C}\varepsilon-\text{H}$ (28), $\text{C}_\gamma-\text{C}\delta-\text{H}$ (11)	1236	NtH_3^+ asym. rock. (29), $\text{C}\beta$ -twist. (10)	
	1267 (m)		1225	$\text{C}\beta$ -twist. (32), $\text{C}\varepsilon-\text{C}\alpha-\text{H}$ (30)	
1236 (m)	1223 (m)	$\text{C}\beta-\text{C}\alpha-\text{H}\alpha$ (21), $\text{C}\varepsilon-\text{C}\alpha-\text{H}$ (17), $\text{C}\beta$ -twist. (13)	1225	NtH_3^+ asym. rock. (31), $\text{C}\beta-\text{C}\alpha-\text{H}\alpha$ (17)	
	1191 (sh)	$\text{N}\varepsilon-\text{C}\varepsilon$ (27), $\text{C}_\gamma-\text{N}\varepsilon$ (10), $\text{N}\varepsilon-\text{C}\varepsilon-\text{H}$ (10)	1205	$\text{N}\delta-\text{C}\varepsilon$ (15), $\text{C}_\gamma-\text{N}\varepsilon$ (15), $\text{N}\delta-\text{C}\varepsilon-\text{H}$ (14), $\text{N}\varepsilon-\text{C}\delta-\text{H}$ (11), $\text{C}\gamma-\text{C}\delta-\text{N}\varepsilon$ (10)	
1160 (m)	1171 (w)	$\text{C}\beta$ -twist (25), NtH_3^+ asym. rock. (10)	1149	$\text{C}_\gamma-\text{N}\varepsilon$ (15), $\text{C}_\gamma-\text{N}\varepsilon$ (15), $\text{N}\delta-\text{C}\varepsilon-\text{H}$ (11), $\text{C}\gamma-\text{C}\delta-\text{N}\varepsilon$ (10)	
	1141 (w)	NtH_3^+ asym. rock. (38), $\text{C}\varepsilon-\text{C}\alpha-\text{H}$ (20)	1130	$\text{C}_\gamma-\text{N}\varepsilon$ (26), $\text{N}\delta-\text{C}\varepsilon$ (16)	
1108 (w)	1107 (w)	$\text{C}\gamma-\text{N}\varepsilon$ (26), $\text{N}\varepsilon-\text{C}\delta-\text{H}$ (11), $\text{N}\varepsilon-\text{C}\varepsilon$ (11)	1063	$\text{Nt}-\text{C}\alpha$ (34), $\text{C}\alpha-\text{C}\beta$ (21)	
	1091 (m)	$\text{Nt}-\text{C}\alpha$ (25), $\text{C}\alpha-\text{C}\beta$ (16)	1028	$\text{C}\gamma-\text{N}\delta-\text{C}\varepsilon$ (12)	
1071 (m)	1088 (m)				
	1072 (m)				
1048 (sh)	1046				
	1021 (w)				
1010 (sh)	1006	$\text{C}_\gamma-\text{N}\delta-\text{C}\varepsilon$ (17), $\text{N}\delta-\text{C}\varepsilon-\text{N}\varepsilon$ (11)	987	$\text{C}\alpha-\text{C}\beta$ (30), $\text{C}\alpha-\text{C}\varepsilon$ (11)	
	983	$\text{C}\alpha-\text{C}\beta$ (22), $\text{C}\beta$ -wag. (20)	965	$\text{C}\beta$ -wag. (28), $\text{Nt}-\text{C}\alpha$ (16)	
993 (m)	986 (w)	$\text{C}_\varepsilon-\text{N}\varepsilon-\text{C}\delta$ (23), $\text{C}_\gamma-\text{N}\delta$ (11)	939	$\text{C}\varepsilon-\text{N}\varepsilon-\text{C}\delta$ (37), $\text{N}\delta-\text{C}\varepsilon-\text{N}\varepsilon$ (18)	
	965 (w)	$\text{Nt}-\text{C}\alpha$ (11)	855	$\omega(\text{C}\delta-\text{H})$ (52), $\tau(\text{C}\gamma-\text{C}\delta)$ (12)	
938 (w)	970	$\omega(\text{C}\delta-\text{H})$ (39), $\tau(\text{C}\gamma-\text{C}\delta)$ (12)	826	$\omega(\text{C}\varepsilon-\text{H})$ (81)	
	923 (w)	$\text{C}\alpha-\text{C}\beta$ (11)	818	$\tau(\text{C}\varepsilon-\text{N}\delta)$ (33), $\omega(\text{C}\delta-\text{H})$ (14), $\tau(\text{N}\delta-\text{C}\gamma)$ (10)	
874 (sh)	908		782	OCHO (13), $\text{C}\beta$ -wag (9)	
	886 (w)		736	$\text{C}\beta$ -scissor. (14), $\tau(\text{N}\delta-\text{C}\alpha)$ (11)	
855 (m)	802	$\text{C}\alpha-\text{C}\beta$ (11)	676	$\tau(\text{C}\delta-\text{N}\varepsilon)$ (44), $\tau(\text{N}\varepsilon-\text{C}\varepsilon)$ (26), $\omega(\text{C}\delta-\text{H})$ (10)	
	798	$\omega(\text{C}\varepsilon-\text{H})$ (73)	655	$\omega(\text{N}\delta-\text{H})$ (35), $\tau(\text{N}\varepsilon-\text{C}\varepsilon)$ (11)	
784 (sh)	726				
	715 (w)				
663 (w)	684				
	652				
620 (w)	652				

^a s, intense; m, medium; w, weak; sh, shoulder; Raman, Raman spectra recorded in H_2O buffers (Figure 6); IR, FT-IR spectra recorded in H_2O (Figure 7); Calcd, calculated wavenumbers from the lowest-energy conformers of neutral histidine $\text{His}^0[\text{N}_t\text{H}]$ and $\text{His}^0[\text{N}_d\text{H}]$ interacting with a cluster of seven water molecules (Figure 5 middle and bottom).

TABLE 5: Vibrational Modes of Histidine with Neutral Side Chains in Aqueous Solutions (D_2O) and Their Assignments

Raman	IR	calcd His ⁰ [N _d D]	assignments (PED %)	calcd His ⁰ [N _d D]	assignments (PED %)
1617 (w)	1619 (s)	1669	CtOO ⁻ asym. st. (78)	1669	CtOO ⁻ asym. st. (85), CaCO asym. bend. (11)
1602 (w)	1600	1600	C γ -C δ (38), N ε -C δ -H (15), C β -C γ (13)	1584	C γ -C δ (30), C β -C γ (15), N ε -C δ -H (11), N δ -C γ -C δ (11)
1567 (s)			N δ -C ε (32), N ε -C ε -H (20)	1512	N ε -C ε (24), C β -bend. (14), N δ -C ε -H (11), N ε -C ε -H (10)
1483 (m)	1485 (m)	1527	N δ -C ε (32), N ε -C ε -H (20)	1501	C β -bend. (82)
1441 (m)	1442 (m)	1500	C β -bend. (94)		
1408 (s)	1407 (s)	1422	CtOO ⁻ sym. st. (21), C β -rock. (17), C α -Ct (10),	1433	CtOO ⁻ sym. st. (32), C β -rock. (15), C α -Ct (10)
1374 (s)		1405	N ε -C ε (20), CtOO ⁻ sym. st. (13)	1407	C γ -N δ (27), COO ⁻ sym. st. (11)
		1391	C β -rock. (24), N t -C α -H (19), C β -C α -H (18), C γ -N ε (11)	1390	C β -rock. (38), C β -C α -H (19), CtOO ⁻ sym. st. (10)
			N t -C α -H (42), C β -C α -H (20)	1364	N t -C α -H (42), N t -C α -H (20)
1353 (m)	1353 (sh)	1369	N δ -C ε (20), C β -twist. (15)	1360	N δ -C ε (22), N ε -C ε (17), N δ -C ε -H (11)
1336 (sh)	1337 (m)	1348	N t -C α -H (35), CtOO ⁻ sym. st. (13), Cr-C α -H (11)	1329	C β -C α -H (24), C β -rock. (16), C β -twist. (11)
1319 (s)	1317 (sh)	1298	C β -rock. (28), C β -twist. (13), C γ -N ε (11)		
1278 (s)		1284	C γ -N δ (14), C β -C γ (11), C β -C α -H (11), Ct-C α -H (10)	1275	C γ -C δ -H (19), N ε -C δ -H (18), N δ -C ε -H (10), N ε -C ε -H (10)
1259 (sh)		1278	N δ -C ε -H (18), Ct-C α -H (10)	1262	C γ -N ε (17), N δ -C ε (13)
1232 (m)		1221	NtD ₃ ⁺ asym. bend (15), NtD ₃ ⁺ sym. rock.	1238	NtD ₃ ⁺ asym. bend. (50), W(DOD) (20)
1197 (s)		1207	C β -twist. (29), NtD ₃ ⁺ asym. bend. (16)	1215	C β -twist. (32), Ct-C α -H (11)
1172 (sh)		1184	NtD ₃ ⁺ asym. bend. (25), NtD ₃ ⁺ sym. rock. (17), NtD ₃ ⁺ sym. rock. (16)		
1107 (sh)		1147 (w)	C γ -N ε (21), N ε -C ε (20), N ε -C ε -H (12)	1140	C γ -N ε (41), N ε -C δ -H (22)
1098 (s)		1108 (w)	1127		
1098 (s)		1097 (w)		1102	C α -C β (44), NtD ₃ ⁺ asym. rock. (11)
1070 (w)		1070	C α -C β (28), Nt-C α (12)		
1038 (w)		1044	C β -wag. (13), C γ -C δ (10)	1038	Nt-C α (16), C β -wag. (16), C β -C α -Ct (11)
1005 (sh)		1022	C β -wag. (10), Nt-C α -C β (10), Nt-C α (10)	1033	Nt-D ₃ ⁺ asym. rock. (22), NtD ₃ ⁺ asym. rock. (20), Nt-C α -Ct (10), Ct-C α -H (10)
991 (s)				1008	C γ -N δ -C ε (15), C γ -N δ (12)
973 (sh)					C ε -N ε -C δ (35), N δ -C ε -N ε (20), N δ -C ε -H (10)
923 (w)	952 (w)	988	NtD ₃ ⁺ asym. rock. (20), C β -C α -Ct (12)	936	C ε -N ε -C δ (35), N δ -C ε -N ε (20), N δ -C ε -H (10)
		944	C ε -N ε -C δ (25), N δ -C ε -N ε (17), C δ -N ε -D (13)	915	C ε -N δ -D (20), C γ -N δ -D (13), N δ -C ε (11)
		917	C ε -N ε -D (32), C δ -N ε -D (10)	895	C β -wag. (33), NtD ₃ ⁺ asym. rock. (13)
			C β -wag. (25), Nt-C α (10)		
873 (w)		889	ω (C δ -H) (46), τ (C γ -C δ) (12)		
863 (w)		879	ω (C δ -H) (46), τ (C γ -C δ) (12)	865	NtD ₃ ⁺ asym. rock. (20), C α -Ct (11), OCtO (11)
		870	NtD ₃ ⁺ asym. rock. (23), C α -C β (18)	842	ω (C δ -H) (44)
				840	ω (C δ -H) (26), NtD ₃ ⁺ asym. rock. (10), C α -C β (10)
816 (s)		816	NtD ₃ ⁺ asym. rock. (12), Nt-C α (11)	824	ω (C ε -H) (88), τ (N ε -C ε) (10)
777 (w)		799	ω (C ε -H) (69)		
		796	ω (C ε -H) (10), C β -scissor. (10), C α -C β (10)	769	C β -wag. (11), τ (Nt-C α) (10), OCtO (10)
			τ (C ε -N δ) (26), C β -scissor. (13), τ (C δ -N ε) (10)	727	C β -scissor. (20), τ (C δ -N ε) (13)
717 (w)		729	τ (C ε -N δ) (19), C β -C ε (15)	680	δ (C δ -N ε) (37), τ (N ε -C ε) (33)
665 (m)		681	ω (N ε -D) (28), τ (N ε -C ε) (14), τ (C δ -N ε) (12)	653	ω (N δ -D) (15), τ (C ε -N δ) (14)
626 (w)		647		596	ω (N δ -D) (33)
608 (sh)		852 (w)			

^a S, intense; m, medium; w, weak; sh, shoulder; Raman, Raman spectra recorded in D₂O (Figure 6); IR, FT-IR spectra recorded in D₂O (Figure 7); Calcd, calculated wavenumbers obtained from the lowest-energy conformers of protonated histidine interacting with a cluster of seven water molecules (Figure 5 middle and bottom).

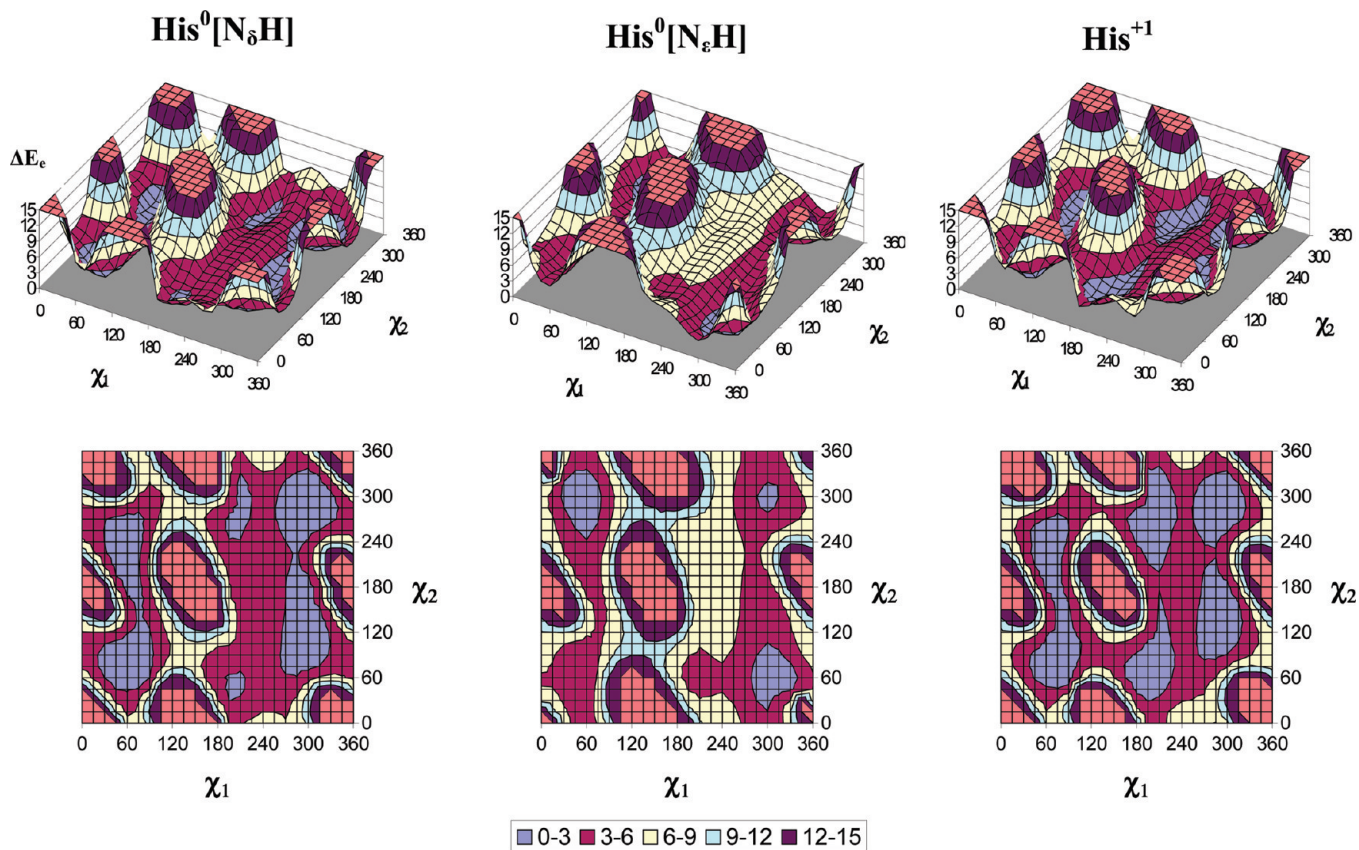


Figure 2. 3D (top row) and 2D (bottom row) representations of potential energy surfaces showing the variation of electronic energy (E_e) of histidine, embedded in a dielectric continuum, as a function of the conformational angles χ_1 and χ_2 (Figure 1). The deepest valleys of these PESs are in blue.

COO^- group. Another conformer of His^{+1} with a g^-g^- conformation is separated by only 0.07 kcal/mol from the lowest-energy one (Table 1). $\text{His}^0[\text{N}_\delta\text{H}]$'s lowest conformer is g^-g^+ , presenting a favorable interaction of N_δ with the backbone NH_3^+ group (Figure 3 middle). This conformer is separated by 0.51 kcal/mol (Table 1) from another g^+g^- conformer. Finally, the lowest-energy conformer of $\text{His}^0[\text{N}_\delta\text{H}]$ is a g^-g^- one, favoring, as can be seen in Figure 3 bottom, the interaction of the whole imidazolic ring with the backbone NH_3^+ group. Other low-energy conformers of $\text{His}^0[\text{N}_\delta\text{H}]$ are separated by at least 1 kcal/mol from the lowest-energy one (Table 1).

III.3. Search of Low Energy Conformers of Histidine Interacting Explicitly with a Cluster of n Water Molecules.

III.3.1. Histidine + Three Water Molecules. In all cases, the three water molecules form generally a trimer bound to NH_3^+ at one side and to COO^- at the other for maintaining the zwitterionic character of the backbone. It is evident that this small number of hydration cannot adequately solvate all H-bond donors and acceptors of histidine. Table 1 reports the main features of a set of representative low-energy conformers located in a 10 kcal/mol interval from the lowest-energy one. In Figure 4 are displayed the lowest-energy conformers, with tg^- , g^-g^+ , and g^+g^+ conformations for His^{+1} , $\text{His}^0[\text{N}_\epsilon\text{H}]$, and $\text{His}^0[\text{N}_\delta\text{H}]$ species, respectively. Note that a g^+g^+ conformer gives rise to a very compact configuration (Figure 4 bottom) favoring the interaction of water molecules bound to the backbone, with N_δH and N_ϵ sites of the imidazolic ring. This is the main difference with the lowest-energy conformers of His^{+1} (Figure 4 top) and $\text{His}^0[\text{N}_\epsilon\text{H}]$ (Figure 4 middle) which render possible the intramolecular H-bonding of N_δH or N_δ , either with the COO^- or with the NH_3^+ groups of the backbone, respectively.

III.3.2. Histidine + Seven Water Molecules. The number of hydration, $n = 7$, corresponds exactly to that of H-bond donor and acceptor sites of histidine. Consequently, a better solvation of the AA is expected by this cluster of water molecules. Table 1 provides the main features of the low energy conformers in a 10 kcal/mol interval. As in the other cases described above (His + continuum and His + 3 H_2O), the tg^- conformer, with a specific H-bond interaction of $\text{N}_\epsilon\text{H}$ with one of the hydrating water molecules (Figure 5 top), is found to be the most energetically favorable of His^{+1} . $\text{His}^0[\text{N}_\epsilon\text{H}]$ and $\text{His}^0[\text{N}_\delta\text{H}]$ lowest-energy conformers are of g^-g^- and tg^- types, respectively (Figure 5 middle and bottom). They are different from those obtained in the case of His + continuum (Figure 3 middle and bottom) and His + 3 H_2O (Figure 4 middle and bottom).

III.4. Energy Difference between the Histidine Forms with Neutral Side Chains. As previously suggested²⁸ and also confirmed by the present calculations (Table 1), among the species with neutral side chains, $\text{His}^0[\text{N}_\epsilon\text{H}]$ is energetically more favorable as compared with $\text{His}^0[\text{N}_\delta\text{H}]$. Histidine tautomerism was subject to numerous discussions based on the results obtained by means of different spectroscopic techniques—¹³C, ¹⁵N, and ¹H NMR and Raman scattering^{44–46,28}—leading to the determination of $\text{His}^0[\text{N}_\epsilon\text{H}]/\text{His}^0[\text{N}_\delta\text{H}]$ relative populations, depending on the backbone $\text{NH}_2/\text{NH}_3^+$ protonation state. All these studies have concluded that the population of $\text{His}^0[\text{N}_\epsilon\text{H}]$ tautomer dominates in aqueous solution.

To estimate the value of the energy difference, $(\Delta E)^{0,0}$, separating the two neutral tautomers, we have used the theoretical results described in the three preceding sections (Table 1)

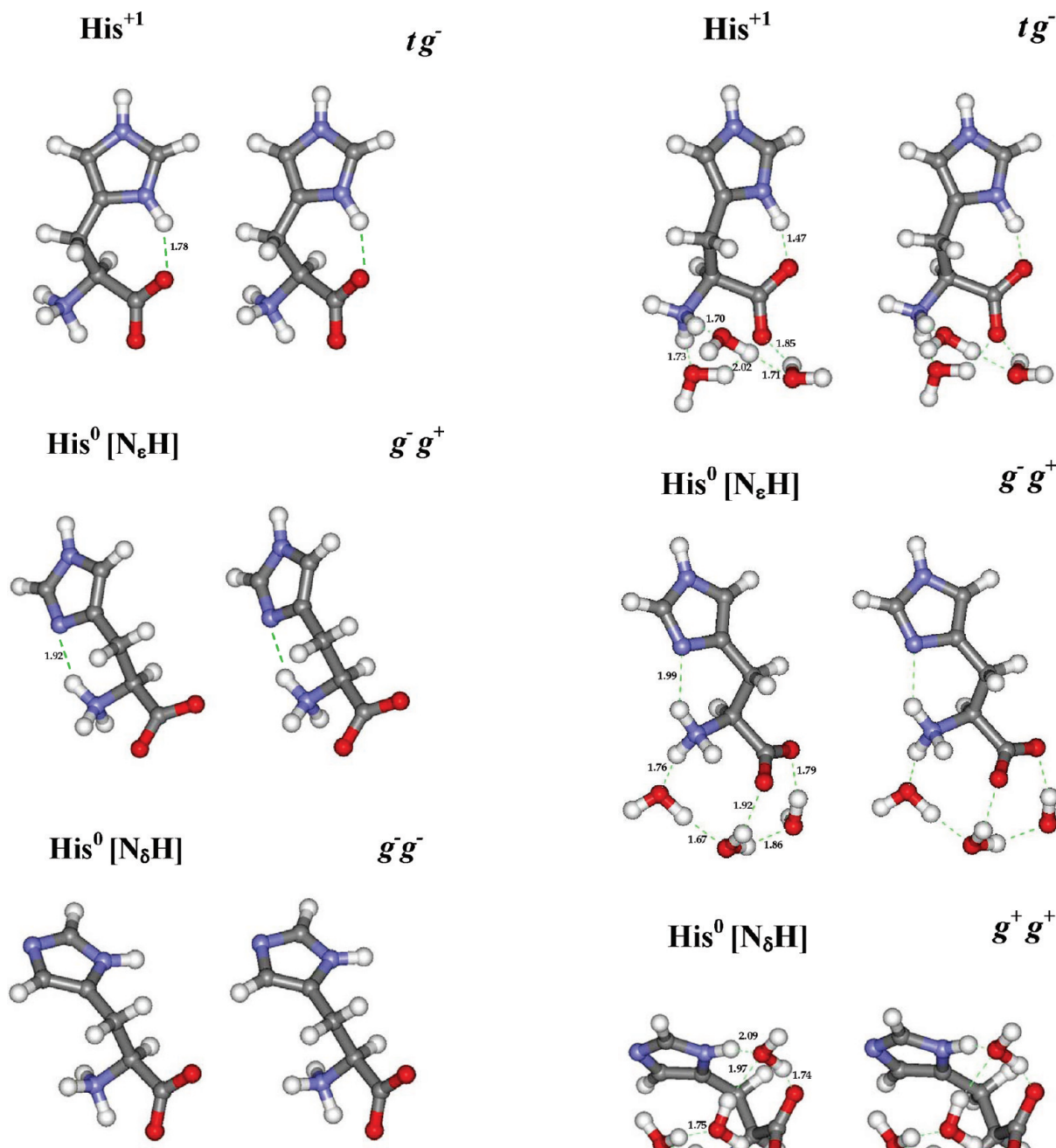


Figure 3. Streoviews of the lowest-energy conformers of histidine with protonated and neutral side chains, as optimized in a polarizable dielectric medium. The conformation of each form, corresponding to the values of χ_1 and χ_2 angles, is reported at the right side of each view. See Table 1 and text for details. H-bonds are drawn with green broken lines, and their lengths are reported in angströms.

and considered two different manners for evaluating $(\Delta E)^{0,0}$, as follows,

$$\text{Estimate 1: } (\Delta E^{0,0})_1 = [E_{\min}]_{N\delta H} - [E_{\min}]_{N\epsilon H}$$

$$\text{Estimate 2: } (\Delta E^{0,0})_2 = [E_{\min} + \langle \Delta E \rangle]_{N\delta H} - [E_{\min} + \langle \Delta E \rangle]_{N\epsilon H}$$

where $E = E_{\text{tot}} = E_e + E_v$, the sum of electronic and vibrational energies, the subscript “min” designates the lowest energy evidenced by theoretical calculations, and $N\delta H$ and $N\epsilon H$ refer to $\text{His}^0[N\delta H]$ and $\text{His}^0[N\epsilon H]$ forms, respectively. $\langle \Delta E \rangle$ is the

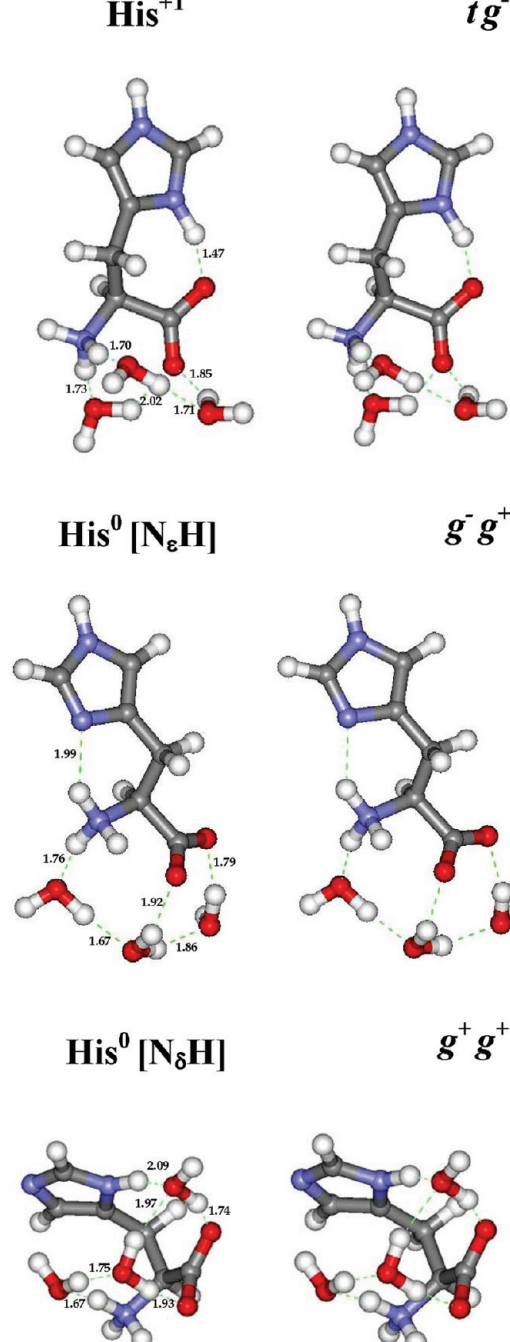


Figure 4. Streoviews of the lowest energy conformers of histidine with protonated or neutral side chains, as optimized in the presence of 3 water molecules. The conformation of each form, corresponding to the values of χ_1 and χ_2 angles, is reported at the right side of each view. See Table 1 and text for details. H-bonds are drawn with green broken lines, and their lengths are reported in angströms.

Boltzmann thermal average at $T = 300$ K ($RT \approx 0.6$ kcal/mol) over all the ΔE values corresponding to the low energy conformers revealed by theoretical calculations (Table 1). The consideration of $\langle \Delta E \rangle$ is, in fact, the main difference between the two types of estimates.

Table 6 shows the values of $(\Delta E^{0,0})_1$ and $(\Delta E^{0,0})_2$ estimated by theoretical calculations with implicit and explicit hydrations. Main conclusions derived from these estimates can be described as follows: (i) Implicit or explicit hydrations give rise to close values of $(\Delta E^{0,0})_2$ and $(\Delta E^{0,0})_1$. This means that the main part of the estimated energy difference comes from $(\Delta E^{0,0})_1$. (ii) The

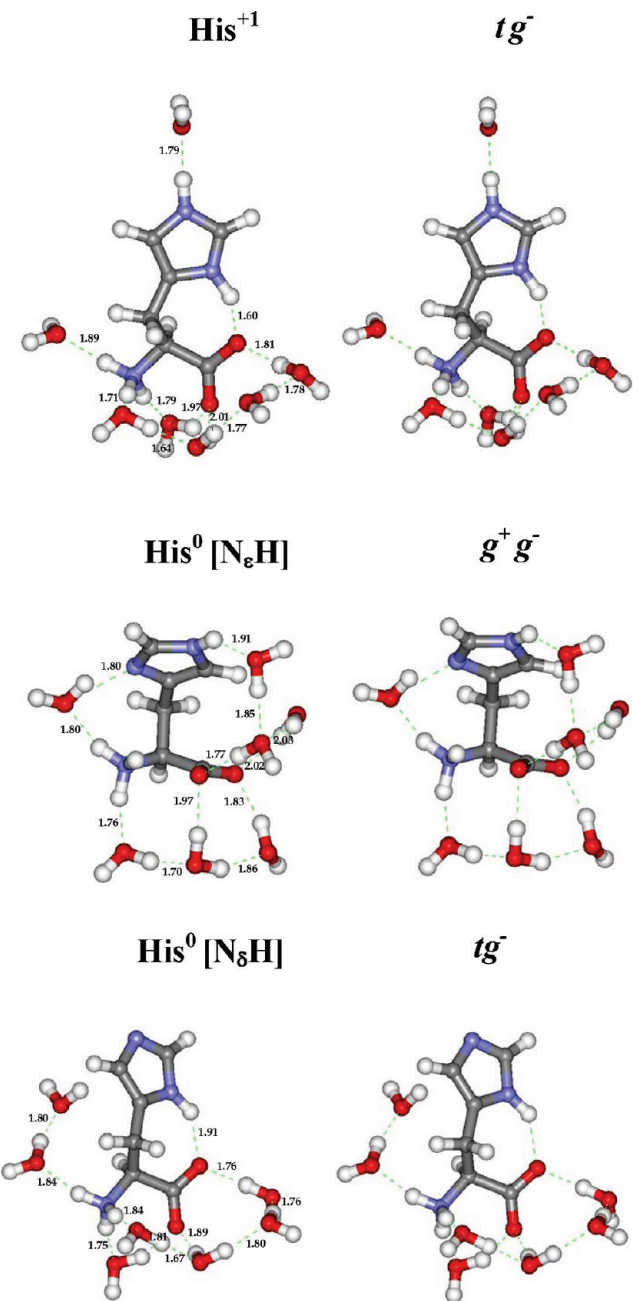


Figure 5. Stereoviews of the lowest-energy conformers of histidine with protonated or neutral side chains, as optimized in the presence of seven water molecules. The conformation of each form, corresponding to the values of the χ_1 and χ_2 angles, is reported at the right side of each view. See Table 1 and text for details. H-bonds are drawn with green broken lines, and their lengths are reported in angstroms.

TABLE 6: Estimates of the Energy Difference Separating the Two Histidine Forms with Neutral Side Chains^a

	His + continuum	His + 3H ₂ O	His + 7H ₂ O
($\Delta E^{0,0}$) ₁ ^b	3.04	2.60	3.84
($\Delta E^{0,0}$) ₂ ^c	3.19	2.66	3.96

^a Values are in kcal/mol. ^b ($\Delta E^{0,0}$)₁ = [E_{\min}]_{NδH} - [E_{\min}]_{NεH}. ^c ($\Delta E^{0,0}$)₂ = [E_{\min} + $\langle \Delta E \rangle$]_{NδH} - [E_{\min} + $\langle \Delta E \rangle$]_{NεH}.

smallest estimates correspond to the calculations with three water molecules. As mentioned above, in His + 3H₂O calculations, not all donor and acceptor sites are adequately solvated. See, for instance, the lowest-energy conformers in Figure 4. (iii) Comparable estimates are provided by the calculations in a

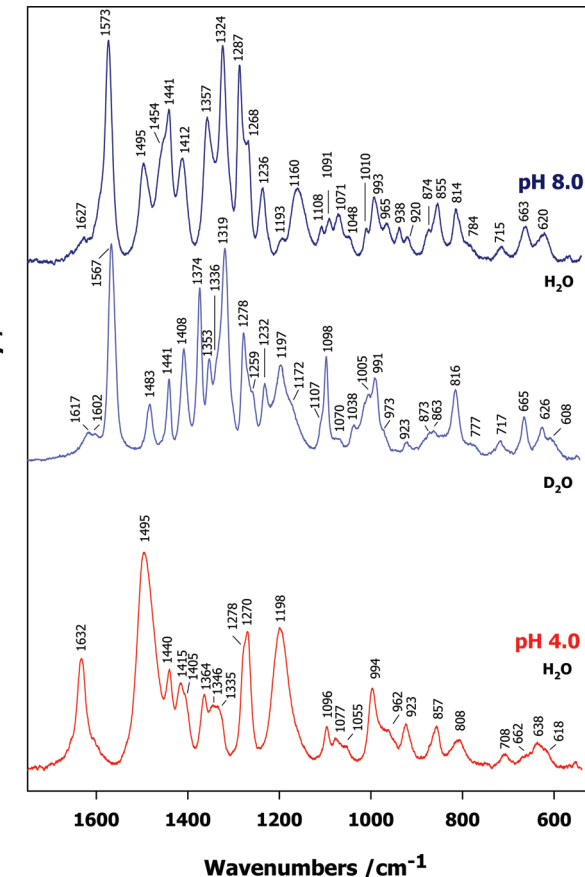


Figure 6. Raman spectra ($\lambda_L = 488$ nm) of histidine observed in aqueous solutions at room temperature. Top: spectrum recorded in H₂O buffer at pH 8. Middle: spectrum recorded in D₂O buffer. Bottom: spectrum recorded in H₂O buffer at pH 4. The intensity of each observed spectrum was normalized to its most intense peak.

solvent continuum or in the presence of seven water molecules, ranging between 3 and 4 kcal/mol.

III.5. Vibrational Data. III.5.1. Calculated Vibrational Wavenumbers with Implicit and Explicit Hydrations. In a recent paper devoted to lysine and arginine,²³ we opened the discussion on the influence of hydration model on the high wavenumber vibrational modes, sensitive to hydration. As shown in Table 2, the explicit hydration leads to large shifts in a number of vibrational modes arising from N–H and C–O bond stretching modes. These shifts do not generally improve the agreement between the calculated and observed wavenumbers. For this reason, the general tendency in the literature is to conclude that the implicit hydration is a more adequate model for reproducing vibrational spectra. As we will discuss later on, this type of conclusion does not seem to be valid upon consideration of the overall spectral region including middle and low wavenumbers.

III.5.2. Assignment of the Observed Vibrational Spectra at pH 4 and 8. Taking into account the pK_a of histidine side chain, the vibrational spectra recorded at pH 8 should contain mainly the forms with neutral side chains (i.e., His⁰[N₈H] and His⁰[N_eH]), whereas those at pH 4 correspond to the form with a protonated side chain (i.e. His⁺¹) (Figures 6 and 7). We have also reported in the same figures the vibrational spectra observed in D₂O (pD 8), corresponding to the neutral forms deuterated on labile hydrogens (NH₃⁺, N₈–H or N_e–H). In Table 3, comparison was made between the observed and calculated wavenumbers corresponding to His⁺¹ form. To emphasize the influence of the hydration models (implicit or explicit), the theoretical wavenumbers obtained from the full geometry optimized conformers of His⁺¹ in a solvent

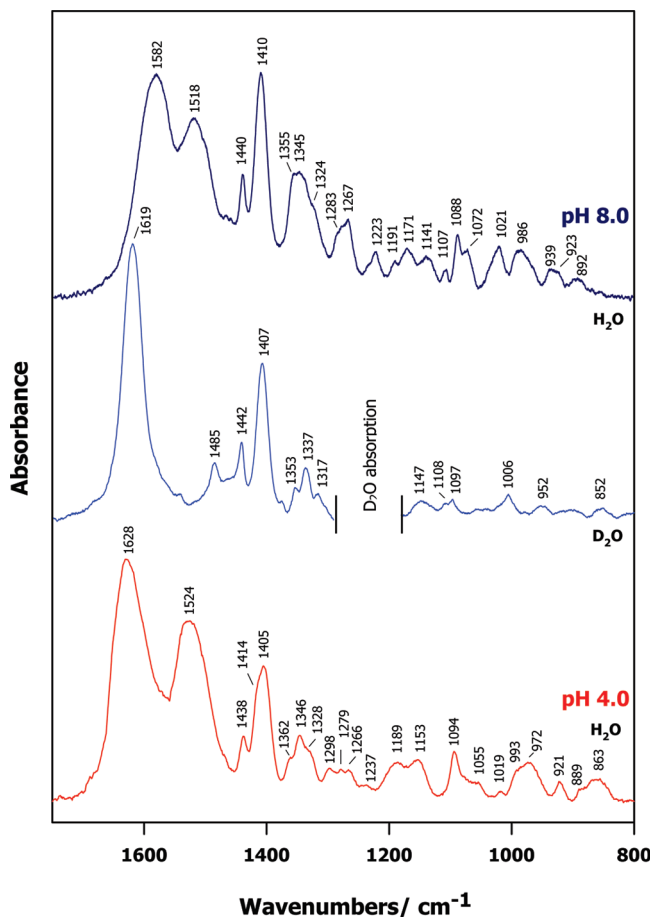


Figure 7. Fourier transform infrared absorption (FT-IR) spectra of histidine observed in aqueous solutions at room temperature. Top: spectrum recorded in H_2O buffer at pH 8. Middle: spectrum recorded in D_2O buffer. Because of the difficulties encountered for its subtraction by means of a numerical procedure, the very intense $1290\text{--}1190\text{ cm}^{-1}$ IR band (D_2O bending mode), was removed. Bottom: spectrum recorded in H_2O buffer at pH 4. The intensity of each observed spectrum was normalized to its most intense peak.

continuum (Figure 3) or in the presence of $7\text{H}_2\text{O}$ (Figure 5), were compared in Table 3. A better distribution of the calculated modes with explicit solvent is obtained in the whole spectral region observed by Raman (R) and IR measurements (Figures 6 and 7). Especially, they can assign satisfactorily the most intense bands observed at pH 4 (i.e. those located at 1632 (R), 1628 (IR), 1524 (IR), 1495 (R), 1278–1270 (R), 1198 (R) cm^{-1}) to the protonated side chain ring. Tables 4 and 5 show the comparison between the observed (at pH 8 and pD 8) and calculated (from the full geometry optimized conformers of $\text{His}^0[\text{N}_\delta\text{H}]$ and $\text{His}^0[\text{N}_\epsilon\text{H}]$ interacting with $7\text{H}_2\text{O}$) wavenumbers. On the basis of this comparison, we can deduce that the modes arising from both neutral forms are necessary for assigning as accurately as possible the observed vibrational modes. For instance, the intense bands at 1582 (IR) and 1573 (R), might arise from the side chains of $\text{His}^0[\text{N}_\epsilon\text{H}]$ and $\text{His}^0[\text{N}_\delta\text{H}]$ species, respectively. Idem, for the bands at 1518 (IR), 1495 (R) cm^{-1} . In contrast to what have been postulated previously,²⁸ both $\text{His}^0[\text{N}_\epsilon\text{H}]$ and $\text{His}^0[\text{N}_\delta\text{H}]$ might contribute to the Raman bands observed at 1287 and 1268 cm^{-1} . In other words, these modes cannot be considered as the markers of $\text{His}^0[\text{N}_\epsilon\text{H}]$ and $\text{His}^0[\text{N}_\delta\text{H}]$ species, respectively.

III.5.3. Determination of the Relative Populations of Neutral and Protonated Side Chains at pH 6.8; Side Chain pK_a Estimated on the Basis of Raman Spectra. As recalled in section I, one of the most important physicochemical features

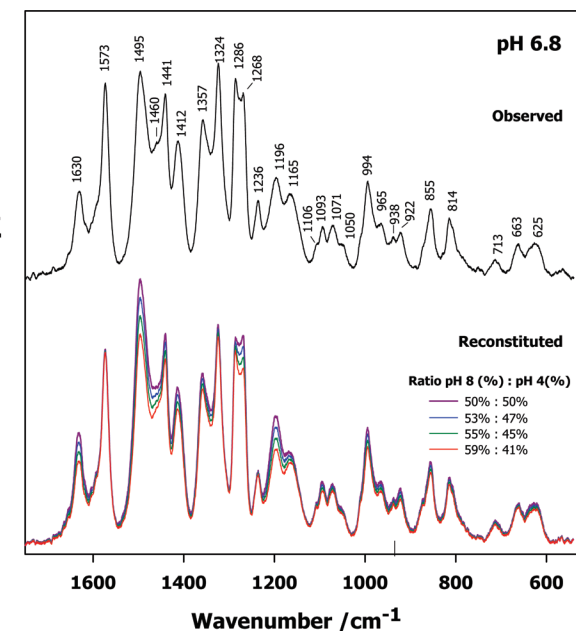


Figure 8. Top: Room temperature Raman spectrum ($\lambda_L = 488\text{ nm}$) of histidine recorded in H_2O buffer at pH 6.8. Bottom: Reconstituted Raman spectra by linear combinations of Raman spectra recorded at pH 8 and 4 (Figure 6 top and bottom). Reconstituted spectra are drawn in different colors together with their corresponding coefficients of linear combination.

of histidine is that at pH values in the physiological range, its side chain can be in neutral and protonated states. In other words, $\text{His}^0[\text{N}_\delta\text{H}]$, $\text{His}^0[\text{N}_\epsilon\text{H}]$, and His^{+1} species might all be present in aqueous solutions. In Figure 8, top, we have displayed the aqueous solution Raman spectrum of histidine recorded at room temperature at pH 6.8. We can easily verify in this spectrum the coexistence of the main Raman bands observed at pH 4 and pH 8 (Figure 6 top and bottom). In Figure 8, bottom, we have shown how a linear combination of the Raman spectra at pH 4 and pH 8 (Figure 6) allows us to reasonably reconstitute that corresponding to pH 6.8. The best fit was obtained for the relative weights of $\sim 60\%$ and 40% considered for the combination of the Raman spectra at pH 8 and 4, respectively. Considering that these estimated weights may represent the relative concentrations of neutral and protonated forms in aqueous solution at pH 6.8 (namely, $[\text{His}^0]$ and $[\text{His}^{+1}]$), respectively, and assuming that $pK_a = \text{pH} - \log\{[\text{His}^0]/[\text{His}^{+1}]\}$, we obtain a reasonable estimate of $pK_a = 6.6$ for the first ionization of the side chain imidazolic ring.

IV. Concluding Remarks

The results obtained by the combined experimental-theoretical protocol described above, has allowed us (i) to propose for the first time a complete set of assignments to the aqueous solution vibrational spectra of histidine observed in the 4–8 pH range; (ii) to show how at an intermediate pH (for instance, 6.8), one can determine the relative populations of histidine forms with protonated and neutral side chains by means of Raman spectra; (iii) to evidence by means of quantum mechanical calculations the role of the two conformational angles, χ_1 and χ_2 , on the energy of different histidine forms (indeed, the cooperative variation of these angles permits optimization of the side chain ring exposure to the solvent and ligands); and (iv) to estimate the energy difference separating the two histidine forms with neutral side chains (Table 6). In fact, this energy difference is comparable to that generally assigned to a medium strength

H-bond (3–4 kcal/mol). As a consequence, the enthalpy variation estimated previously upon temperature dependence of Raman spectra,²⁸ $\Delta H = 1.0 \pm 0.3$ kcal/mol, seems to be surprisingly low and should thus be reconsidered. In conclusion, we can consider that the energy loss in going from His⁰[N_eH] to His⁰[N_δH] neutral tautomers may be compensated in solution by the interaction of N_e atom with solvent, surrounding molecules, or with metal ions. Further experiments accompanied presumably by theoretical calculations seem to be necessary for analyzing the proton transfer dynamics from His⁰[N_eH] to His⁰[N_δH] in aqueous solution at pH values in the physiological range.

Acknowledgment. This work, based on a consequent amount of numerical calculations, could not have been realized without the computational facilities on the Jade (SGI) supercomputing network. The authors thank the GENCI-CINES (Montpellier, France) for the calculation time assigned to the scientific application involving the quantum mechanical calculations on histidine.

Supporting Information Available: Atomic Cartesian coordinates of the lowest energy conformers of histidine with protonated and neutral side chains obtained from the full geometry optimization in the presence of implicit or explicit solvent (see Figures 3–5 of the text) are provided. This material is available free of charge via the Internet at <http://pubs.acs.org>.

References and Notes

- (1) Reeds, P. J. *J. Nutr.* **2000**, *130*, 183S–40S.
- (2) Fürst, P.; Stehle, P. *J. Nutr.* **2000**, *134*, 1558S–1565S.
- (3) Kendrew, J. C.; Bodo, G.; Dintzis, H. M.; Parrish, R. G.; Wyckoff, H.; Phillips, D. C. *Nature* **1958**, *181*, 662–666.
- (4) Kendrew, J. C.; Dickerson, R. E.; Strandberg, B. E.; Hart, R. G.; Davies, D. R.; Phillips, D. C.; Shore, V. C. *Nature* **1960**, *185*, 422–427.
- (5) Gibson, J. F.; Ingram, D. J.; Perutz, M. F. *Nature* **1956**, *178*, 906–908.
- (6) Perutz, M. F.; Rossmann, M. G.; Cullis, A. F.; Muirhead, H.; Will, G.; North, A. C. *Nature* **1960**, *185*, 416–422.
- (7) Di Cera, E. *IUMB Life* **2009**, *61*, 510–515.
- (8) Berg, J. M.; Tymoczko, J. L.; Stryer, L. *Biochemistry*, 5th ed.; Freeman W. H. & Co.: San Francisco, 2002.
- (9) Garret, R.; Grisham, C. *Biochemistry*, 3rd ed.; Thomson-Brooks-Cole: Beklmont, CA, 2005.
- (10) Matthews, B. W.; Sigler, P. B.; Henderson, R.; Blow, D. M. *Nature* **1967**, *214*, 652–656.
- (11) Blow, D. M.; Birktoft, J. J.; Hartley, B. S. *Nature* **1969**, *221*, 337–340.
- (12) Page, M. D.; Di Cera, E. *Cell. Mol. Life Sci.* **2008**, *65*, 1220–1236.
- (13) Rawlings, N. D.; Barrett, A. J. *Methods Enzymol.* **1994**, *244*, 19–61.
- (14) Polgár, L. *Cell. Mol. Life Sci.* **2005**, *62*, 2161–2172.
- (15) Dementin, S.; Belle, V.; Bertrand, P.; Guigliarelli, B.; Adryanczyk-Perrier, G., L.; De Lacey, A.; Fernandez, V. M.; Rousset, M.; Léger, C. J. *Am. Chem. Soc.* **2006**, *128*, 5209–5218.
- (16) Mus-Veteau, I.; Guerlesquen, F. *Biochem. Biophys. Res. Commun.* **1994**, *201*, 128–134.
- (17) Volbeda, A.; Charon, M. H.; Piras, C.; Hatchikian, E. C.; Frey, M.; Fontecilla-Camps, J. C. *Nature* **1995**, *373*, 580–587.
- (18) Guiffo-Soh, G.; Hernández, B.; Coic, Y. M.; Boukhalfa-Heniche, F. Z.; Ghomi, M. *J. Phys. Chem. B* **2007**, *111*, 12563–12572.
- (19) Guiffo-Soh, G.; Hernández, B.; Coic, Y. M.; Boukhalfa-Heniche, F. Z.; Fadda, G.; Ghomi, M. *J. Phys. Chem. B* **2008**, *112*, 1282–1289.
- (20) Hernández, B.; Carelli, C.; Coic, Y. M.; De Coninck, J.; Ghomi, M. *J. Phys. Chem. B* **2009**, *113*, 12796–12803.
- (21) Derbel, N.; Hernández, B.; Pfleider, F.; Liquier, J.; Geinguenaud, F.; Jaïdane, N.; Ben Lakhdar, Z.; Ghomi, M. *J. Phys. Chem. B* **2007**, *111*, 1470–1477.
- (22) Hernández, B.; Pfleider, F.; Nsangou, M.; Ghomi, M. *J. Phys. Chem. B* **2009**, *113*, 3169–3178.
- (23) Hernández, B.; Pfleider, F.; Derbel, N.; De Coninck, J.; Ghomi, M. *J. Phys. Chem. B* **2010**, *114*, 1077–1088.
- (24) Petrosyan, A. M. *Vibr. Spectrosc.* **2007**, *43*, 284–289.
- (25) Barth, A. *Prog. Biophys. Mol. Biol.* **2000**, *74*, 141–173.
- (26) Wolpert, M.; Hellwig, P. *Spectrochim. Acta A* **2006**, *64*, 987–1001.
- (27) Mesu, J. G.; Visser, T.; Soulimani, F.; Weckhuysen, B. M. *Vibr. Spectr.* **2005**, *39*, 114–125.
- (28) Ashikawa, I.; Itoh, K. *Chem. Lett.* **1978**, *7*, 681–684.
- (29) Hudáky, P.; Beke, T.; Perczel, A. *J. Mol. Struct. (THEOCHEM)* **2002**, *583*, 117–135.
- (30) Hudáky, P.; Hudáky, I.; Perczel, A. *J. Mol. Struct. (THEOCHEM)* **2002**, *583*, 199–213.
- (31) Hudáky, P.; Perczel, A. *J. Phys. Chem. A* **2004**, *108*, 6195–6205.
- (32) Hudáky, P.; Perczel, A. *J. Mol. Struct. (THEOCHEM)* **2004**, *675*, 117–127.
- (33) Láng, A.; Füzéry, A. K.; Beke, T.; Hudáky, P.; Perczel, A. *J. Mol. Struct. (THEOCHEM)* **2004**, *675*, 163–175.
- (34) Kohn, W.; Sham, L. *J. Phys. Rev.* **1965**, *140*, A1133–A1138.
- (35) Becke, A. D. *J. Chem. Phys.* **1993**, *98*, 5648–5652.
- (36) Lee, C.; Yang, W.; Parr, R. G. *Phys. Rev. B* **1988**, *37*, 785–789.
- (37) Frisch, M. J.; Trucks, G. W.; Schlegel, H. B.; Scuseria, G. E.; Robb, M. A.; Cheeseman, J. R.; Montgomery, J. A., Jr.; Vreven, T.; Kudin, K. N.; Burant, J. C.; Millam, J. M.; Iyengar, S. S.; Tomasi, J.; Barone, V.; Mennucci, B.; Cossi, M.; Scalmani, G.; Rega, N.; Petersson, G. A.; Nakatsuji, H.; Hada, M.; Ehara, M.; Toyota, K.; Fukuda, R.; Hasegawa, J.; Ishida, M.; Nakajima, T.; Honda, Y.; Kitao, O.; Nakai, H.; Klene, M.; Li, X.; Knox, J. E.; Hratchian, H. P.; Cross, J. B.; Bakken, V.; Adamo, C.; Jaramillo, J.; Gomperts, R.; Stratmann, R. E.; Yazyev, O.; Austin, A. J.; Cammi, R.; Pomelli, C.; Ochterski, J. W.; Ayala, P. Y.; Morokuma, K.; Voth, G. A.; Salvador, P.; Dannenberg, J. J.; Zakrzewski, V. G.; Dapprich, S.; Daniels, A. D.; Strain, M. C.; Farkas, O.; Malick, D. K.; Rabuck, A. D.; Raghavachari, K.; Foresman, J. B.; Ortiz, J. V.; Cui, Q.; Baboul, A. G.; Clifford, S.; Cioslowski, J.; Stefanov, B. B.; Liu, G.; Liashenko, A.; Piskorz, P.; Komaromi, I.; Martin, R. L.; Fox, D. J.; Keith, T.; Al-Laham, M. A.; Peng, C. Y.; Nanayakkara, A.; Challacombe, M.; Gill, P. M. W.; Johnson, B.; Chen, W.; Wong, M. W.; Gonzalez, C.; Pople, J. A. *Gaussian 03, Revision C.02*, Gaussian, Inc.: Wallingford, CT, 2004.
- (38) Barone, V.; Cossi, M. *J. Phys. Chem. A* **1998**, *102*, 1995–2001.
- (39) Cossi, M.; Rega, G.; Scalmani, G.; Barone, V. *J. Comput. Chem.* **2003**, *24*, 669–681.
- (40) Wang, W.; Pu, X.; Zheng, W.; Wong, N. B.; Tian, A. *J. Mol. Struct. (THEOCHEM)* **2003**, *626*, 235–244.
- (41) Ramaekers, J.; Pajak, J.; Lambie, B.; Maes, G. *J. Chem. Phys.* **2004**, *120*, 4182–4193.
- (42) Balta, B.; Aviyente, V. *J. Comput. Chem.* **2003**, *24*, 1789–1802.
- (43) Balta, B.; Aviyente, V. *J. Comput. Chem.* **2004**, *25*, 690–703.
- (44) Reynolds, W. F.; Peat, I. R.; Feedman, M. H., Jr. *J. Am. Chem. Soc.* **1973**, *95*, 328–331.
- (45) Kawano, K.; Kyogoku, Y. *Chem. Lett.* **1975**, *4*, 1305–1308.
- (46) Blomberg, F.; Mauer, W.; Ruterjans, H. *J. Am. Chem. Soc.* **1977**, *99*, 8149–8159.

JP103348Y